J Nanostruct 15(1): 168-179, Winter 2025

RESEARCH PAPER

The Impact of Gallium Dopant on the Structure, Surface Morphology, Optical Band Gap and Photoluminescence Properties of ZnO-Polystyrene Nanocomposites

*Sajjad Ali Ameen [1], Mahmood Salim Karim [1], Adel H. Omran Alkhayatt [2,3]**

[1] College of Education, Mustansiriyah University, Baghdad, Iraq

[2] Faculty of Science, University of Kufa, Najaf, Iraq

[3] College of Health and Medical Technology, University of Alkafeel, Najaf, Iraq

ARTICLE INFO

Article History:
Received 21 September 2024
Accepted 28 December 2024
Published 01 January 2025

Keywords:
Ga dopant
Hydrothermal
Photoluminescence
PS composites
ZnO:Ga NPs

ABSTRACT

The study details the synthesis of un-doped and gallium-doped zinc oxide (GZO) (2, 4 and 6) wt% nanoparticles (NPs) via the hydrothermal approaches at a reaction temperature and time of 160 °C and 5 hours respectively. Furthermore, ZnO-polystyrene (PS) and GZO-PS nanocomposite (NCs) films were fabricated using the casting method. The results of X-ray diffraction revealed that both ZnO-PS and GZO-PS nanocomposite films exhibit polycrystalline structures of the ZnO hexagonal wurtzite phase. A broad and low-intensity peak was observed at diffraction angles of approximately (15-23)° related to the noncrystalline peak of polystyrene polymer. The crystalline size and the microstrain were determined utilize the Scherrer and Williamson-Hall methods, showing an increase (26-34) nm and variation with the rise in Ga content. The presence of functional groups in polymer systems was confirmed through (FTIR) spectral analysis. The topographical characteristics of the prepared nanocomposite films indicated that both the roughness and root mean square (r.m.s) roughness increased from 1.89 to 2.31 nm and from 1.54 to 1.87 nm, respectively, with an increase in Ga dopant content. The surface morphology of Zn-PS and GZO-PS nanocomposites revealed nanostructured grains formed by agglomerated particles in the samples. Additionally, varying Ga dopant content altered the density and shape of these unstructured grains. The particle sizes were determined from the corresponding FESEM images, which were about 42 and 46 nm for ZnO-PS and GZO-PS nanocomposites respectively. The GZO-PS nanocomposite clearly demonstrated that the particles are well dispersed within the PS polymeric compounds. The optical absorption edge of ZnO-PS red-shifted and the forbidden direct energy band gap reduced from 4.4 eV to 3.74 eV at a Ga content of 6 wt %. Furthermore, photoluminescence studies of the produced nanocomposite films demonstrated bright blue light emission. The incorporation of GZO nanoparticles into a polystyrene (PS) matrix led to the formation of a nanocomposite exhibiting continuous and intense blue emissions. The integration of GZO nanoparticles into a PS matrix resulted in the creation of a nanocomposite that displays continuous and vibrant blue emissions.

How to cite this article
Ameen S., Karim M., Alkhayatt A. The Impact of Gallium Dopant on the Structure, Surface Morphology, Optical Band Gap and Photoluminescence Properties of ZnO-Polystyrene Nanocomposites. J Nanostruct, 2025; 15(1):168-179. DOI: 10.22052/JNS.2025.01.016

* *Corresponding Author Email: adilh.alkhayat@uokufa.edu.iq*

INTRODUCTION

Zinc oxide (ZnO) is a fascinating semiconductor recognized for its excellent electrical conductivity and high transmittance in the visible spectrum, demonstrating potential as a material for diverse applications across fields, including lasers, light-emitting diodes (LEDs), solar cells, and sensors [1,2]. Recently, there has been considerable interest in oxide-based semiconducting materials owing to their practical implementations in light-emitting diodes, displays, and scintillators. The first radiation detectors with various uses were scintillators, luminous materials. They were fundamentally depended on in several fields, including inspection, medical radiography, geophysical exploration, clear medicine, diagnostics, and dosimetry [1]. ZnO is a wide direct energy gap (3.37 eV) semiconductor with a high density and bright light at room temperature. It is usually found in the shape of a hexagonal crystal (wurtzite). When used as a radiation detector, it will glow and perhaps boost light production, particularly when doped with an activator. Gallium doped the hexagonal ZnO lattice creates a cluster of unsteady electrons and substrates around the minimum band gap conduction states. This makes the scintillation qualities of the host structure better [3, 4, 5]. Because the majority of scintillators are available in brittle crystal or granular form, which restricts their applications, polymer-based scintillator composites comprised of scintillator nanoparticles and polymer have been developed. For instance, Polystyrene is a noteworthy polymer that finds extensive application as a transparent matrix due to its cost-effectiveness, flexibility, stability as a binder matrix, and resistance to thermal, radiation, and light degradation. Therefore, great focus is paid to the development of polymer scintillation composites, which are inexpensive and simpler to create than single-crystal growth techniques [6]. The comparatively low deposition temperatures during manufacture, along with cheap material prices, have drawn interest in gallium-doped zincoxide (ZnO:Ga) films [7].

S. Alamdari et al. [8] synthesized ZnO and Ga-doped ZnO (GZO)/polystyrene (PS) nanocomposite films, along with luminescent nanoparticles produced via the sol–gel method. Photoluminescence and ionoluminescence studies of the prepared nanoparticles demonstrated a blue emission. The combination of GZO NPs into a PS molecules series leads to the producing of a nanocomposite exhibiting intense blue emission. The findings suggested that GZO/PS NCs could serve as a worthy scintillation material for radiation detection applications. Many studies showed that the GZO/polystyrene nanocomposite is significant for radiation detection. H. Buresova, [9] investigated the ZnO:Ga-PS nanocomposite for its ultrafast subnanosecond decay. The nanocomposite was created by integrating the ZnO:Ga NPs into the PS matrix. Additionally, the ZnO:Ga NPs was synthesized through photo-induced precipitation, followed by annealing in air and Ar/H_2 atmospheres. The ZnO:Ga-PS NCs was produced by mixing the NPs powder of a 10 wt% fraction with polystyrene and compressing the mixture using a press to form a particle with a thickness of 1 mm. These flexible, user-friendly plastic foils enhance fast timing capabilities when paired with an additional rapid, high-yield inorganic light burst. Concerning further studies in this field, R. M. Sahani et al. [10] revealed that by employing ZnO:Ga vertically aligned nanorods on glass substrate with diameter of about 150 ± 10 nm was successfully detected as yielded by UV-Vis spectroscopy, band gap value of around 3.22 eV, which is in agreement with the photoluminescence near band emission observation of 393 nm. Q. Li et al. [11] conducted another investigation in which it was discussed that a ZnO:Ga microds - epoxy (ZnO:Ga-EP) composite was required for high energy physics experimental facilities' ultra-fast and hard X-ray imaging and detection. Accordingly, for successful production ZnO:Ga-EP composite by using hydrothermal polymerization procedure. Shiyi He and et al. [12] made a significant advancement in enhancing the luminescence intensity of hydrothermally grown Ga-doped ZnO single crystals. This breakthrough was accomplished by applying $CsPbBr_3$-dodecyl benzene sulfonic acid (DBSA) quantum dots to the surface of the GZO crystal. By coating $CsPbBr_3$ QD films on both sides, the photoluminescence intensity was enhanced to 2.43 times that of GZO. Notably, the ratio of emitted light from GZO was found to be fewer than 6%. This innovative approach holds promise for further advancements in the field of luminescent materials and their applications. To investigate the potential employments and implications of ZnO-PS and ZnO:Ga-PS thin scintillators, it is essential to produce them employing an easy and

flexible method to guarantee a thickness of less than 1 mm. Numerous experimental attempts to produce ZnO film have been documented to date, including pulsed laser deposition (PLD) [13], M. sputtering [14], atomic layer deposition (ALD) [15], thermal evaporation in vacuum [16], and plasma-enhanced molecular beam epitaxy [17], chemical bath deposition (CBD) [18] and by plasma-enhanced chemical vapor deposition (PECVD) [19]. In the present work, Ga-doped ZnO nanoparticles are novel synthesized by hydrothermal method at low reaction time and low reaction temperature, as well as the ZnO: Ga-PS nanocomposites synthesized by casting approach. The impact of Ga dopant content on the crystal structure, surface topography, surface morphology, photoluminescence and optical characterization was investigated for different sensing and radiation detection applications.

MATERIALS AND METHODS

ZnO and GZO powder nanoparticles were synthesized using the hydrothermal method. Zinc acetate dihydrate $Zn(CH_3COO)_2 \cdot 2H_2O$ and gallium nitrate $Ga(NO_3)_3 \cdot xH_2O$ served as precursor materials. Three grams of zinc acetate were dissolved in 75 ml of distilled water (DW) while stirring for 15 minutes; 2.4 g of sodium hydroxide NaOH was dissolved in 75 ml of DW and stirred for another 15 minutes. Then the NaOH solution gradually added to the Zn acetate solution. After 30 minutes of constant stirring, a white gelatinous solution was generated. The prepared solution was transferred it in to the Teflon-lined stainless steel autoclave (40 ml) and heated 160 °C for 5 hours after in an oven. White precipitated was found, centrifuged three times at 5000 rpm for 15 minutes. Finally the obtained with zinc oxide (ZnO) powder was dried at heated at 90 °C for 1 hour. The same procedure was repeated after adding Ga dopant (2, 4 and 6) wt % for synthesis of ZnO:Ga nanoparticles. In the second step, 2 g of polystyrene was dissolved in 30 ml of toluene with stirring for 3 hours. Un-doped and Ga-doped ZnO nanoparticles were efficiently pulverized before their addition to the polymer solution; 0.5 g of the prepared NPs was dissolved in 5 ml of toluene and stirred at an elevated rotational speed for three more hours. An appropriate amount of pre-prepared ZnO-PS and GZO-PS solutions were drop casting on glass substrates and left to dry at room temperature. The polymer mixture films separated readily after 24 hours. The structural characteristics, FTIR analysis, topographical, morphological, optical and photoluminescence characterization of the synthesized nanocomposite materials were performed by X-ray diffraction (XRD), using a PANalytical PW3050/60 diffractometer, Fourier transform infrared spectrophotometer (FT-IR) Alpha-Brukar (Germany), Atomic force microscopy (AFM), (TT-2 AFM Workshop, USA/ SPM), field emission scanning electron microscope (FESEM-TESCAN MIRA3), double beam Mega 2100 Sinco. UV-Vis spectrophotometer and PerkinElmer LS-5 Fluorescence Spectrometer respectively.

RESULTS AND DISCUSSION

Structure analysis

The synthesized ZnO-PS and GZO-PS nanocomposites crystal structure were analyzed using X-ray diffraction from their diffraction patterns as in Fig. 1. The diffraction patterns exhibits polycrystalline structure of the hexagonal wurtzite phase of ZnO lattice structure. The diffraction peaks were observed at diffraction angles 30.8°, 33.4°, 35.2°, 46.6°,55.6°, 61.8°, 65.4°, 67.0°, 68.0°, 71.6° and 76.2°, which correspond to the (100), (002), (101) ,(102), (110), (103), (200), (112), (201), (004) and (202) diffraction respectively. The preferred orientation is along (101) plane at $2\theta = 35$. A board peak was observed at about (15-23)° attribute to polystyrene indicate to the semicrystalline of polystyrene polymer, the result is consistent with [20, 21]. The diffraction patterns of the ZnO-PS nanocomposite approve the successful integration of ZnO NPs into polystyrene structure [22, 23]. It was observed that in the presence of polystyrene, the ZnO peaks shift towards the lower angles as compared with the standard pattern. The obtained results are consistent with the results of S. Alamdari et al. [8], M. Yilmaz et al. [24] and Q. Li et al. [11]. The diffraction peaks intensity decreased after ZnO NPs doped by Ga at different content (2, 4 and 6) wt% which can be attributed to the replacement of Zn^{+2} ions of radius 0.074 nm by smaller Ga^{+3} ions of radius 0.047nm [8, 13]. Any further peaks for strange cluster or impurity peaks were not detected in ZnO-PS and GZO-PS samples which confirm the formation of a single phase hexagonal wurzite ZnO structure. As well as any shift in the diffraction peaks was not observed at different angle with presence and increase of Ga dopant content as shown in Fig. 2. a and c constants of

ZnO hexagonal lattice were determined using the d_{hkl} spacing relation for the (hkl) Miller indices plane [22, 25]:

$$\frac{1}{d_{hkl}^2} = \frac{4}{3}\left(\frac{h^2+hk+k^2}{a^2}\right) + \frac{l^2}{c^2} \quad (1)$$

The lattice constant a was found to be about 3.341 to 3.355 Å for ZnO-PS and GZO-PS and the lattice contant c was found to be about 5.361 to 5.363 Å for ZnO-PS and GZO-PS composites as illustrated in Table 1, which well matched with standard values. The crystallite size D of the prepared nanocomposites ZnO-PS and GZO-PS was calculated using Debye Scherrer's equation [24]:

$$\left(D = \frac{0.9\lambda}{\beta\cos\theta}\right) \quad (2)$$

The average crystallite size be approximately 21.4-21.5 nm, respectively, when θ represents the diffraction angle, λ the wavelength of the used x-ray = 1.5406 Å, β denotes the intensity of the

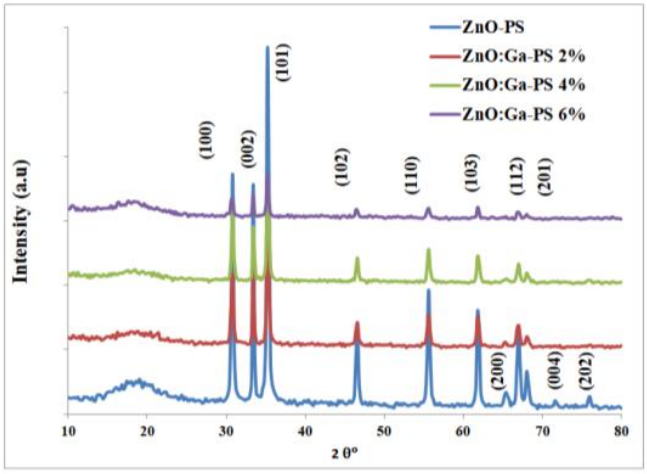

Fig. 1. X-ray diffraction patterns of ZnO/PS and ZnO:Ga/PS nanocomposites.

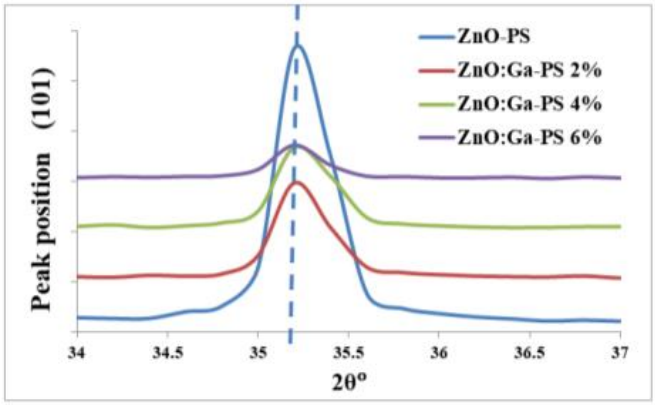

Fig. 2. The (101) diffraction peak as a consequence of ZnO/PS GZO/PS nanocomposites.

full width at half maximum ascribed to the (101) plane.

The micro strain ε was calculated depending on Shererre equation using the relation [8]:

$$\varepsilon = \frac{\beta \cos\theta}{4} \quad (3)$$

The lattice strain of ZnO-PS nanocomposite is 1.60×10^{-3} indicating the presence of lattice deformation and this strain increases as the Ga dopant content increased to about 1.617×10^{-3} at 6% of Ga content GZO-PS nanocomposite. The increase in Ga dopant concentration creates more defects and more imperfections in the ZnO lattice. From Fig. 2, the (101) peak position fixed without any shift, so one can conclude that the GZO lattice strain is a nonuniform strain, where the strain affect the peak position, the peak broadening and intensity which were called uniform and nonuniform strain respectively [26, 27].

The dislocation density δ was determined using the following equation [28]:

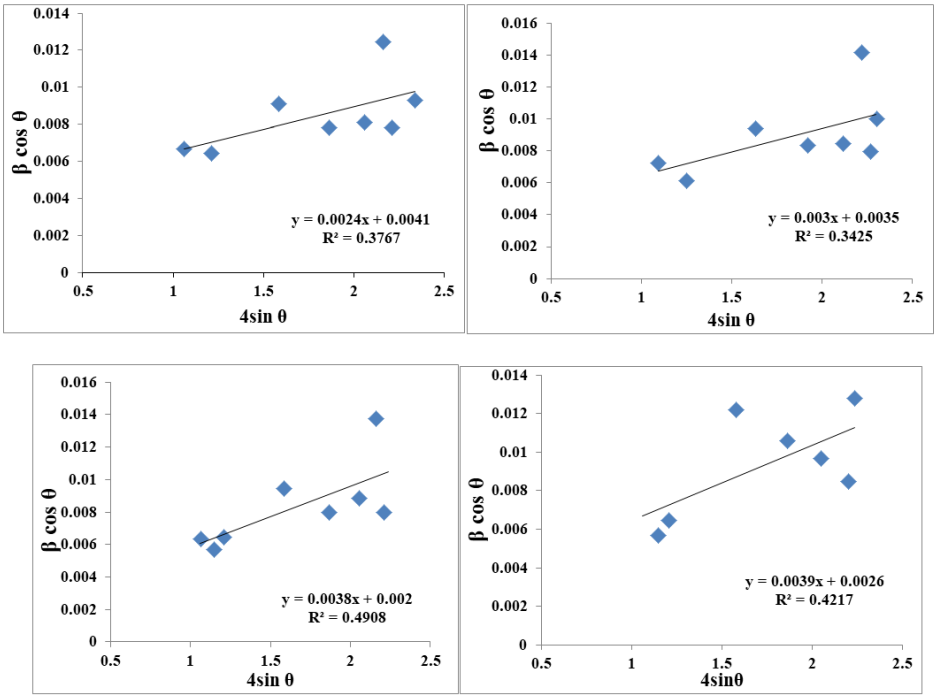

Fig. 3. W-H plot of βcosθ versus 4sinθ for a. ZnO-PS and b.2%, c.4% and d. 6% GZO-PS.

Table 1. Structure parameters of ZnO-PS and GZO-PS nanocomposites.

ZnO:Ga-PS % Sample	d_{xrd} (Å)	d_{ICPDS} (Å)	a (Å)	c (Å)	$D_{sherrer}$ (nm)	D_{W-H}	$\delta_{sh}\times10^{15}$ Line/m²	$\delta_{W-H}\times10^{15}$ Line/m²	ε_{sh}	ε_{W-H}
0	2.544	2.4759	3.341	5.361	21.5512	26.1611	2.153	1.461	0.001608	0.0024
2	2.5443	2.4759	3.352	5.361	22.5489	28.8862	1.967	1.198	0.001537	0.003
4	2.5436	2.4759	3.349	5.33	21.4383	34.6635	2.176	0.832	0.001617	0.0038
6	2.5466	2.4759	3.355	5.363	21.43582	30.812	2.176	1.053	0.001617	0.0039

$$\delta = \frac{1}{D^2} \quad (4)$$

The dislocation density of ZnO lattice is about 2.153×10^{15} line/m^2 and increased to 1.79×10^{15} line/m^2 at Ga dopant content of 6% as illustrated in Table 1. These results explain and confirm the effects of lattice dislocations in the crystallite boundaries which produced from the integration of G^{+3} ions in ZnO lattice [11, 16, 21]. The diffraction peak widening is a result of the effect of the size and the strain which can be offered from XRD analysis. Williamson-Hall (W–H) method can differentiate clearly between the broadening effects from the size of the crystal and the micro-strain [26]. So, the total peak widening according to the lattice strain and the particles or the crystallite size of hkl values, can be pointed out as [26, 28]:

$$\beta_{hkl} = \beta_{size} + \beta_{strain} \quad (5)$$

$$\beta_{hkl} = \frac{k\lambda}{D}.\frac{1}{\cos\theta} + 4\varepsilon.\tan\theta \quad (6)$$

From Eq. 6 we get:

$$\beta_{hkl}.\cos\theta = \frac{k\lambda}{D} + 4\epsilon.\sin\theta \quad (7)$$

The plotting of equation (7), with (β_{hkl}.cosθ) versus (4Sinθ) for each diffraction peak of ZnO-PS and GZO-PS NCs illustrated in Fig. 3. The intrinsic

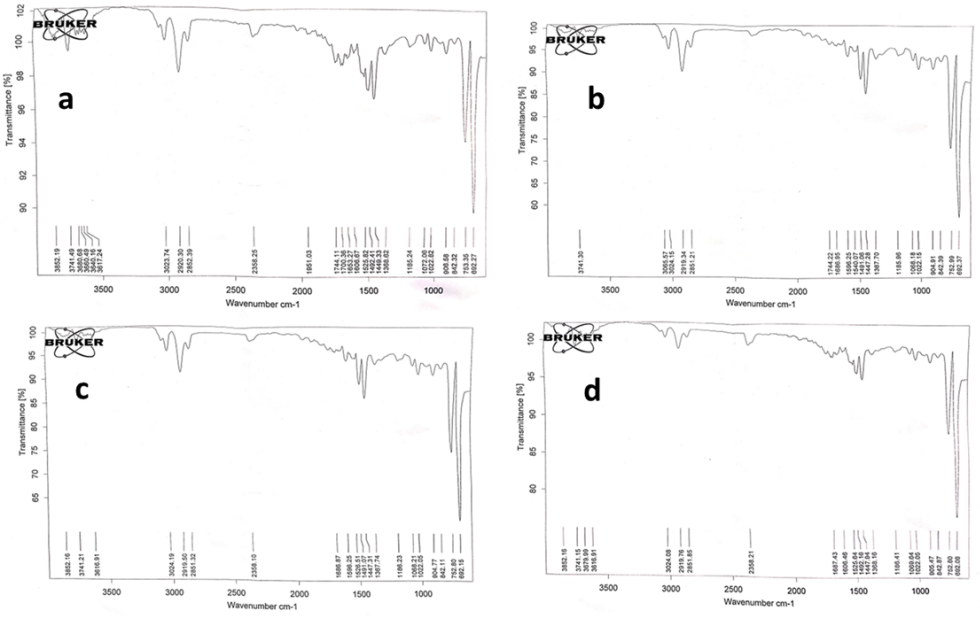

Fig.4. FT-IR transmission spectra of a. ZnO-PS and b. ZnO:Ga2%-PS c. ZnO:Ga4%-PS and d. ZnO:Ga6%-PS nanocomposites.

Table 2. FTIR analysis report results.

ZnO:Ga-PS Ga content %	vibration bands of aromatic C=C (cm^{-1})	asymmetric and symmetric stretching vibrations of $–CH_2$ (cm^{-1})	aromatic C-H stretching vibration (cm^{-1})
0	1525.82 , 1482.41 , 1440.33	3023.74 , 2852.39	3617.24
2	1596.25 , 1540.07 , 1447.28	3024.15 , 2851.21	3741.30
4	1596.25 , 1526.51 , 1491.07	3024.19 , 2851.32	3616.91
6	1606.84 , 1525.84 , 1482.18	3024.08 , 2851.85	3616.91

strain value was found from slope of the straight line, whereas the crystallite size of the prepared samples was determined from the intercept. Equation (7) represents the Uniform Deformation Model (UDM), which assumes that the strain is distributed across the crystal lattice. The obtained value of the lattice strain is positive (Table 1) and rises (2.4-3.9) $\times 10^{-3}$ as Ga content increases to 6 wt%. Where the positive and negative strain represents a tensile and a compressive stress respectively. The ZnO-PS and GZO-PS NCs exhibit positive strain, indicating tensile stress in our NC samples. As Ga is integrated into the ZnO lattice, the observed strain increases, consistent with the results obtained from Scherer's equation, as shown in Table 1.

Investigations of FT-IR spectroscopic

The ZnO-PS nanocomposite FT-IR spectra are depicted in Fig. 4 and Table 2. The FT-IR spectra exhibit absorption at (1750 - 1350) cm^{-1}, indicative of aromatic C=C vibration bands from styrene molecules. The symmetric and asymmetric stretching vibrations of the $–CH_2$ group result in absorption maxima at 3030 and 2860 cm^{-1}. The absorption bands observed in the range of 3750 to 3030 cm^{-1} are associated with the stretching vibration of aromatic C-H bonds. More Over, The spectrum showed many high intensity peaks in the range 400–780 cm^{-1}, related to the hexagonal ZnO and GZO confirms the consistences of ZnO nanoparticles where the main peak of GZO nanoparticles in GZO-PS nanocomposites film was observed at 419-762 cm^{-1}. The results were consistent with previous studies [8, 12, 14, 24-29].

Surface topography

The topographical properties of the prepared ZnO-PS and GZO-PS nanocomposite films was examined using atomic force microscopy (AFM)

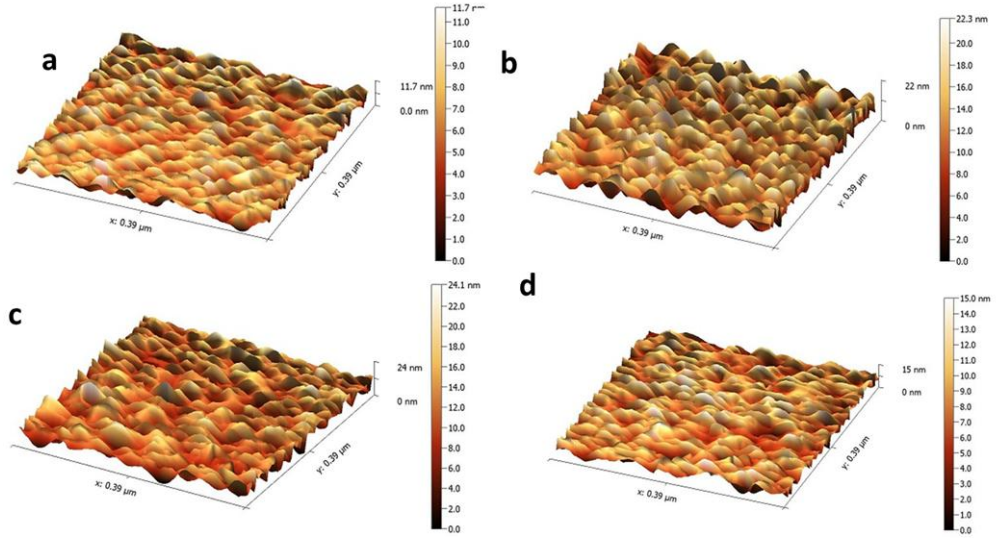

Fig. 5. AFM images of ZnO-polystyrene films at different concentration: (b) ZnO:2%-PS, c. ZnO:Ga4%-PS and d. ZnO:Ga6%-PS.

Table 3. The AFM data of the ZnO-PS and ZnO:Ga-PS nanocomposite films deposited at different Ga dopant content.

ZnO:Ga% Sample	Root maen square (nm)	Average roughness (nm)
O%	1.89	1.54
2%	3.51	2.90
4%	3.39	2.73
6%	2.31	1.87

technique, which is essential for studying the crystal growth mechanization, shape, and the grain size. The AFM images revealed a consistent granular surface with columnar-like grain growth in ZnO-PS and ZnO:Ga-PS films with varying Ga dopant content, as depicted in Fig. 5. An increase in the surface roughness (1.89-2.31) and the root-mean-square (RMS) roughness (1.54-1.87) was observed in the Ga-doped ZnO-PS with (2-6)% dopant content as in Table 3. The surface topography for different dopant content reveals dense surface and the images do not show any changes. The smooth surface was observed for ZnO-PS and an increasing in the Ga content (2 and 4%) to ZnO-PS film appeared with a relatively high surface roughness. Moreover, the RMS surface roughness values indicated a rough surface with an RMS roughness exceeding 1 nm. These results were consistent with the XRD findings. Additionally, AFM analysis demonstrated a good distribution of ZnO nanoparticles within the polymer film. Furthermore, a significant quantity of nanoparticles was observed on the surface of the polystyrene film [12, 30].

Surface morphology

The surface morphology of ZnO-PS and GZO-PS nanocomposites was characterized by field emission scanning electron microscope FESEM as shown Fig. 6. The surface images revealed that this implies nanostructured grains of agglomeration particles in the samples. Additionally, Ga doping concentrations change nanostructured grain density and shape. GZO-PS nanocomposite clearly showed that the NPs are well sparse between PS polymeric molecules. Nanorod-like films formed as Ga doping increased from 2% mol% [31].

Optical properties

The films optical transmittance spectra as shown in Fig. 4 display that the transmittance is towards the long wavelengths, as the absorption edge is in the ultraviolet region. When doped with Ga, we notice that the absorption edge creeps

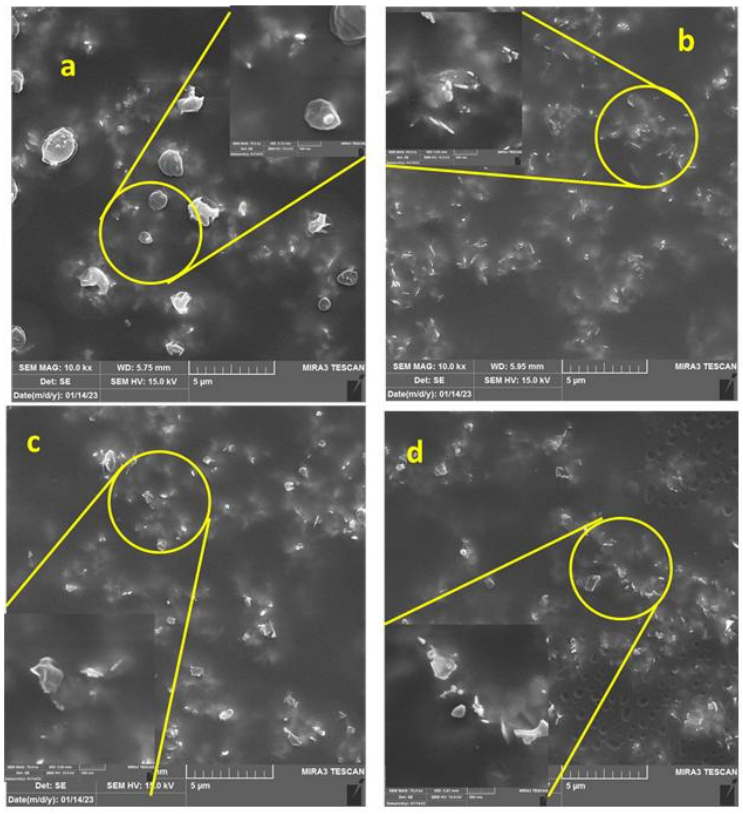

Fig. 6. FESEM images of ZnO:Ga thin films (a) 0 mol% Ga doped, (b)2mol% Ga doped, (c) 4 mol% Ga doped and (d) 6 mol% Ga doped.

towards the long wavelengths (lower energies) because Ga generated morphological defects and found local levels that made the absorption edges shifted towards the low energies, as the absorption increased with the increase in the Ga doping ratio. So that the polystyrene (PS) is suitable material as the host matrix for ZnO:Ga, [14, 15].

From Fig.8, the energy gap was decreased after Ga doping, because Ga generated localized energy levels within the gap, and the energy gap values were found using Tauc plot about 4.44 eV for un-doped ZnO-PS, and 3.91 eV, 3.81 eV , and 3.74 eV for Ga (2, 4and 6)% doped ZnO-PS nanocomposites respectively [15].

Photoluminescence analysis

The PL spectra for ZnO-PS and Ga-doped ZnO-PS nanocomposites are depicted in Fig. 9. The emission of ZnO-PS NC is prominently located at 433 nm, corresponding to the near band edge (NBE) peak, while the band in the visible light region (590 nm) originates from inter-band defects. In Ga-doped ZnO-PS NCs, the blue-green and orange-red emissions diminish with increasing Ga dopant content. The observed UV-blue emission is linked to the recombination of electron-hole carriers.

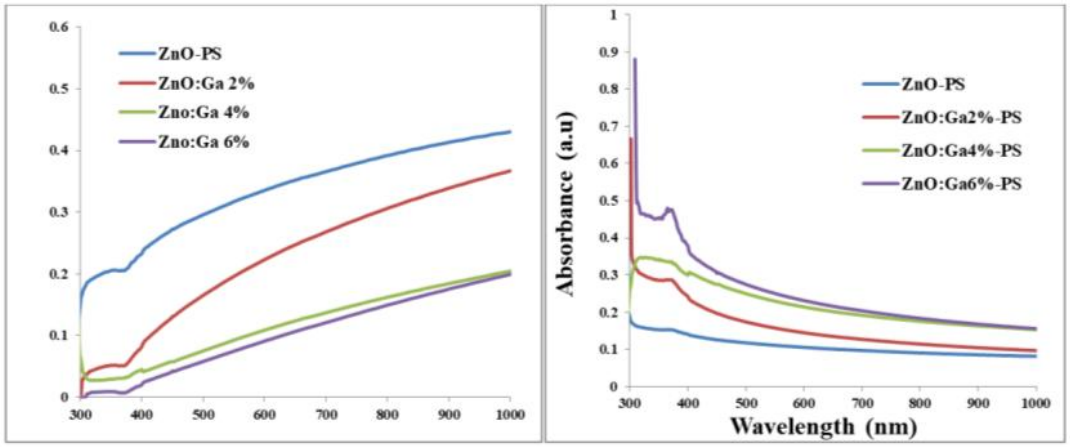

Fig. 7. A. Transmittance and B. absorbance spectrum of ZnO:Ga films.

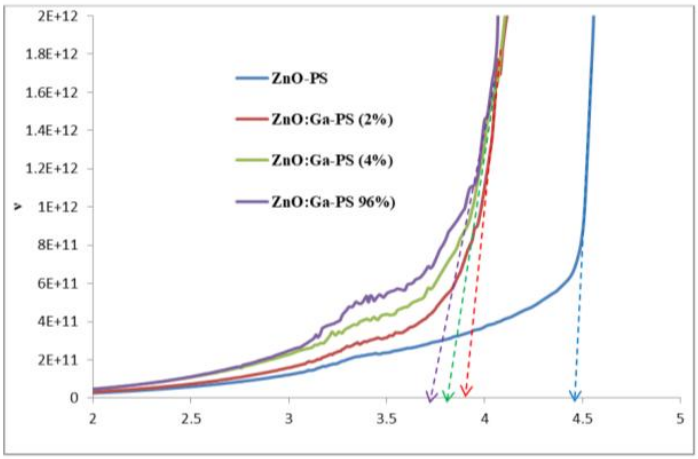

Fig. 8. Energy gap of ZnO:Ga-PS nanocomposites films.

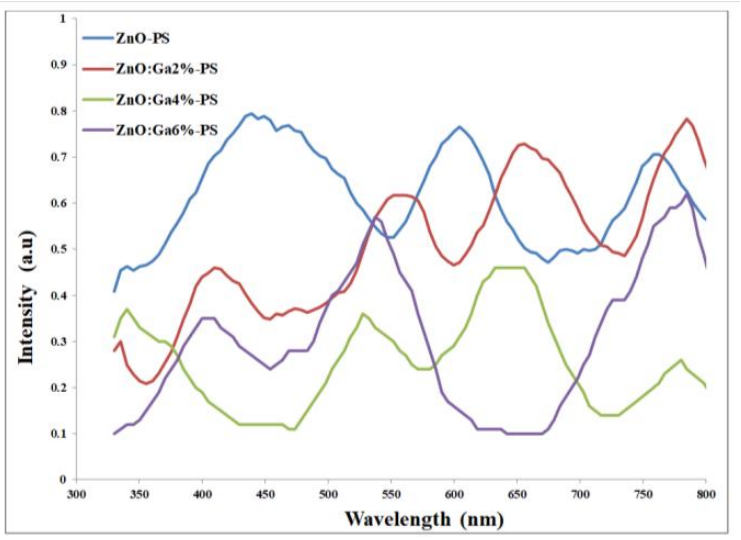

Fig. 9. Photoluminescence spectrum of ZnO-PS and ZnO:Ga-PS nanocomposites for (2, 4 and 6) % Ga dopant content.

The emission peaks in the green-yellow region are associated with the presence of oxygen vacancies and interstitial oxygen states on the surface of the ZnO lattice. For Ga-doped ZnO-PS NCs, both the blue-green and orange-red emissions decrease with higher Ga dopant content. Ga-doping results in a reduction of the emission peaks at 404, 399, and 367 nm for Ga concentrations of 2%, 4%, and 6%, respectively, along with a decline in the green-yellow region emission. This is attributed to the incorporation of Ga atoms into Zn vacancies, which increases the rate of donor-related defects in the ZnO-PS structure. The UV emission peak significantly enhances in GZO, which displays the largest grain size. These findings are consistent with previous studies [8, 14, 15, 31-36]. The observed visible green emissions are primarily due to the oxygen vacancies (Vo), representing a transition between radiation defects associated with interface traps excited at grain boundaries and the valence band. The observed red emissions likely originate from interstitial oxygen (Oi), generated from the conduction band to Oi [8, 28, 34]. Nevertheless, for ZnO:Ga-PS composites, the intensities of all emissions decreased with the presence of the Ga dopant, indicating a reduction in defect states. Thus, the tensile lattice strain observed with Ga doping, as shown by XRD results, does not depend on defect production; it is likely due to the decrease in crystallite size resulting from the growth of ZnO:Ga and the replacement of Ga^{2+} with Zn^{2+}, which have different ionic radii. Similar trends have also been reported in various types of materials [30, 31, 36].

CONCLUSION

Un-doped and Ga (2, 4, and 6) wt% doped ZnO (GZO) nanoparticles were successfully synthesized using the hydrothermal method at 160 °C for 5 hours. Additionally, ZnO-Polystyrene (ZnO-PS) and GZO-PS nanocomposite films were created by drop casting onto a glass plate and drying at room temperature. The structural and surface morphology characterization was conducted based on Ga dopant content. Hexagonal wurtzite ZnO nanoparticle phase was obtained, and the Ga dopant reduced the crystallinity of the prepared nanoparticles while introducing nonuniform strain in the ZnO lattice. The crystallite size and lattice strain were calculated using the Debye-Scherrer equation and W-H methods. The lattice constants a and c were calculated and found to align with standard values. The crystallite size increased with higher Ga content, while the strain also increased with Ga doping, indicating a positive tensile strain. The FESEM images of the prepared ZnO-PS and GZO-PS NCs revealed nanostructured grains of agglomerated particles in the samples. The FTIR spectra exhibited several strong peaks around 400–780 cm^{-1}, corresponding to hexagonal ZnO,

confirming the formation of ZnO nanoparticles, with the main peak of GZO nanoparticles in the GZO-PS nanocomposite film observed at 419-762 cm^{-1}. The AFM images showed a consistent granular surface with columnar-like grain growth in ZnO-PS and ZnO:Ga-PS films with varying Ga dopant content, as depicted in Fig. 5. An increase in surface roughness (1.89-2.31) and root-mean-square (RMS) roughness (1.54-1.87) was observed in the Ga-doped ZnO-PS with (2-6)% dopant content. The energy gap values were determined using the Tauc plot, yielding approximately 4.44 eV for un-doped ZnO-PS, and 3.91 eV, 3.81 eV, and 3.74 eV for Ga (2, 4, and 6)% doped ZnO-PS nanocomposites. The emission of ZnO-PS NC is primarily observed at 433 nm, which corresponds to the near band edge (NBE) peak, while the band in the visible light range (around 590 nm) originates from inter-band defects. In the case of Ga-doped ZnO-PS NCs, both the blue-green and orange-red emissions decrease with increasing Ga dopant content. ZNO-PS and GZO-PS nanocomposites with varying Ga dopant levels, considering structural, surface topography, surface morphology, photoluminescence, and optical results, can be suitable for various sensing and radiation detection applications.

CONFLICT OF INTEREST

The authors declare that there is no conflict of interests regarding the publication of this manuscript.

REFERENCES

1. Schmidt-Mende L, MacManus-Driscoll JL. ZnO – nanostructures, defects, and devices. Mater Today. 2007;10(5):40-48.
2. Ravichandran K, Jabena Begum N, Snega S, Sakthivel B. Properties of Sprayed Aluminum-Doped Zinc Oxide Films—A Review. Mater Manuf Processes. 2014;31(11):1411-1423.
3. Andeen D, Kim JH, Lange FF, Goh GKL, Tripathy S. Lateral Epitaxial Overgrowth of ZnO in Water at 90 °C. Adv Funct Mater. 2006;16(6):799-804.
4. Hamada T, Ito A, Fujii E, Chu D, Kato K, Masuda Y. Preparation of single-crystalline ZnO films on ZnO-buffered a-plane sapphire by chemical bath deposition. J Cryst Growth. 2009;311(14):3687-3691.
5. Janotti A, Van de Walle CG. Fundamentals of zinc oxide as a semiconductor. Rep Prog Phys. 2009;72(12):126501.
6. Al-Fandi M, Oweis R, Albiss BA, AlZoubi T, Al-Akhras MA, Qutaish H, et al. A prototype Ultraviolet Light Sensor based on ZnO Nanoparticles/Graphene Oxide Nanocomposite Using Low Temperature Hydrothermal Method. IOP Conference Series: Materials Science and Engineering. 2015;92:012009.
7. Kubon M, Boehmer E, Siebke F, Rech B, Beneking C, Wagner H. Solution of the ZnO/p contact problem in a-Si:H solar cells. Sol Energy Mater Sol Cells. 1996;41-42:485-492.
8. Alamdari S, Jafar Tafreshi M, Sasani Ghamsari M. Preparation and characterization of gallium-doped zinc oxide/polystyrene nanocomposite scintillator for alpha particles detection. Appl Phys A. 2019;125(6).
9. Burešová H, Procházková L, Turtos RM, Jarý V, Mihóková E, Beitlerová A, et al. Preparation and luminescence properties of ZnO:Ga – polystyrene composite scintillator. Opt Express. 2016;24(14):15289.
10. Sahani RM, Kumari C, Pandya A, Dixit A. Author Correction: Efficient Alpha Radiation Detector using Low Temperature Hydrothermally Grown ZnO:Ga Nanorod Scintillator. Sci Rep. 2020;10(1):3334-3334.
11. Li Q, Yang D, Hao S, An R, Yuan R, Yang Y, et al. Development of the ZnO:Ga microrods - epoxy composite as a scintillation screen for ultrafast X-ray detection. Opt Mater. 2020;102:109805.
12. He S, Zhang S, Wang F, Chen L, Li Y, Ruan J, et al. Enhancement of the luminescence intensity of a ZnO:Ga crystal scintillator via coating CsPbBr3 quantum dot films. Opt Mater. 2024;148:114955.
13. Oga T, Kai R, Kaneko N, Miyazaki H, Kaneko S, Matsuda A, et al. Crystallinity improvement of room-temperature PLD-deposited ZnO thin films on cyclo-olefin polymer substrates subject to surface-pretreatment with vacuum-UV-light irradiation. J Cryst Growth. 2023;603:127012.
14. Song PK, Watanabe M, Kon M, Mitsui A, Shigesato Y. Electrical and optical properties of gallium-doped zinc oxide films deposited by dc magnetron sputtering. Thin Solid Films. 2002;411(1):82-86.
15. Song YS, Seong NJ, Choi KJ, Ryu SO. Optical and electrical properties of transparent conducting gallium-doped ZnO electrodes prepared by atomic layer deposition for application in organic solar cells. Thin Solid Films. 2013;546:271-274.
16. Abdulmunem OM, Mohammed Ali MJ, Hassan ES. Optical and structural characterization of aluminium doped zinc oxide thin films prepared by thermal evaporation system. Opt Mater. 2020;109:110374.
17. Cheng Y-C, Wang H-C, Lai H-C, Shi S-C, Chen C-C, Yao Y-F, et al. Wide range variation of resonance wavelength of GaZnO plasmonic metamaterials grown by molecular beam epitaxy with slight modification of Zn effusion cell temperatures. J Alloys Compd. 2021;870:159434.
18. Ahmed M, Coetsee L, Goosen WE, Urgessa ZN, Botha JR, Venter A. Characterization of Bi-doped ZnO nanorods prepared by chemical bath deposition method. Physica B: Condensed Matter. 2023;666:415105.
19. Johnson KW, Guruvenket S, Sailer RA, Ahrenkiel SP, Schulz DL. Atmospheric pressure plasma enhanced chemical vapor deposition of zinc oxide and aluminum zinc oxide. Thin Solid Films. 2013;548:210-219.
20. Yaseen MW, Asghar MA, Bakhsh EM, Akhtar K, Khan SB, Iqbal M. Plant-mediated synthesis of thermally stable metal-polystyrene nanocomposites for antioxidant and antibacterial food packaging. Industrial Crops and Products. 2024;209:117959.
21. Lam S-M, Chew K-C, Sin J-C, Zeng H, Lin H, Li H, et al. Ameliorated photodegradation performance of polyethylene and polystyrene films incorporated with ZnO-PVP catalyst. Journal of Environmental Chemical Engineering. 2022;10(3):107594.

22. Alwan TJ, Toma ZA, Kudhier MA, Ziadan KM. Preparation and Characterization of the PVA Nanofibers produced by Electrospinning. Madridge Journal of Nanotechnology and Nanoscience. 2016;1(1):1-3.
23. Sahani RM, Pandya A, Dixit A. Zinc oxide/polystyrene composite based scintillator for alpha particle monitoring. Mater Sci Semicond Process. 2021;127:105692.
24. Yilmaz M. Investigation of characteristics of ZnO:Ga nanocrystalline thin films with varying dopant content. Mater Sci Semicond Process. 2015;40:99-106.
25. Ghamsari MS, Alamdari S, Razzaghi D, Arshadi Pirlar M. ZnO nanocrystals with narrow-band blue emission. J Lumin. 2019;205:508-518.
26. Khorsand Zak A, Abd. Majid WH, Abrishami ME, Yousefi R. X-ray analysis of ZnO nanoparticles by Williamson–Hall and size–strain plot methods. Solid State Sciences. 2011;13(1):251-256.
27. Alkhayatt AHO, Jaafer MD, Al Alak HHA, Ali AH. Characterization of CuO/n–Si pn junction synthesized by successive ionic layer adsorption and reaction method. Optical and Quantum Electronics. 2019;51(7).
28. Al Jarrah RM, Kadhem EM, Alkhayatt AHO. Annealing and operating temperatures effect on spray-deposited nanocrystalline ZnO thin-film gas sensor. Appl Phys A. 2022;128(6).
29. Alamdari S, Karkhaneh A, Jafar Tafreshi M, Sasani Ghamsari M. Ultra-thin Hafnium doped ZnO films with enhanced optical transparency and electrical conductivity. Materials Research Express. 2019;6(5):055020.
30. Goktas A, Modanlı S, Tumbul A, Kilic A. Facile synthesis and characterization of ZnO, ZnO:Co, and ZnO/ZnO:Co nano rod-like homojunction thin films: Role of crystallite/grain size and microstrain in photocatalytic performance. J Alloys Compd. 2022;893:162334.
31. Alamdari S, Sasani Ghamsari M, Tafreshi MJ. Novel scintillation properties by entrapping ZnO: Ga nanocrystals in epoxy polymer. Prog Nuclear Energy. 2020;130:103495.
32. Zhao J-H, Liu C-J, Lv Z-H. Photoluminescence of ZnO nanoparticles and nanorods. Optik. 2016;127(3):1421-1423.
33. Shen X, Wei J, Chen L, Wang Z, Hu F, Ouyang Q. Enhancement of nonlinear optical effects of pure and Mn-doped CsPbBr3 perovskite films by external voltage. Opt Mater. 2024;148:114833.
34. Li Q, Liu X, Gu M, Li F, Zhang J, Wu Q, et al. Large enhancement of X-ray excited luminescence in Ga-doped ZnO nanorod arrays by hydrogen annealing. Appl Surf Sci. 2018;433:815-820.
35. Alamdari S, Ghamsari MS, Afarideh H, Mohammadi A, Geranmayeh S, Tafreshi MJ, et al. Preparation and characterization of GO-ZnO nanocomposite for UV detection application. Opt Mater. 2019;92:243-250.
36. Alamdari S, Tafreshi MJ, Ghamsari MS. Strong yellow-orange emission from aluminum and Indium co-doped ZnO nanostructures with potential for increasing the color gamut of displays. Appl Phys A. 2019;125(3).